

## Enhanced processability and electrochemical cyclability of metallic sodium at elevated temperature using sodium alloy composite

Guocheng Li<sup>a</sup>, Qingpeng Yang<sup>a</sup>, Jiale Chao<sup>a</sup>, Bao Zhang<sup>b</sup>, Mintao Wan<sup>a</sup>, Xiaoxiao Liu<sup>a</sup>, Eryang Mao<sup>a</sup>, Li Wang<sup>c</sup>, Hui Yang<sup>d</sup>, Zhi Wei Seh<sup>e</sup>, Jianjun Jiang<sup>b</sup>, Yongming Sun<sup>a,\*</sup>

<sup>a</sup> Wuhan National Laboratory for Optoelectronics, Huazhong University of Science and Technology, Wuhan 430074, China

<sup>b</sup> School of Optical and Electronic Information, Huazhong University of Science and Technology, Wuhan, Hubei, 430074, P.R. China

<sup>c</sup> Institute of Nuclear & New Energy Technology, Tsinghua University, Beijing, 100084, China

<sup>d</sup> State Key Laboratory of Material Processing and Die & Mould Technology, Department of Mechanics, Huazhong University of Science and Technology, Wuhan, Hubei, 430074, P.R. China

<sup>e</sup> Institute of Materials Research and Engineering, Agency for Science, Technology and Research (A\*STAR), 2 Fusionopolis Way, Innovis, Singapore 138634, Singapore

### ARTICLE INFO

#### Keywords:

Na<sub>15</sub>Sn<sub>4</sub>/Na anode  
sodium metal batteries  
processability  
electrochemical performance  
elevated temperature

### ABSTRACT

Na metal batteries have attracted great attention owing to their considerable energy density, abundance of Na resources, and potentially low cost. However, Na metal anode suffers from poor processability and high reactivity, which inhibit its practical applications. Herein, we introduce a cross-linked sodium-tin alloy (Na<sub>15</sub>Sn<sub>4</sub>) network host for metallic Na and fabricated a Na<sub>15</sub>Sn<sub>4</sub>/Na composite foil using a simple cold calendaring approach via spontaneous reaction between metallic Na and metallic Sn, which markedly mitigated the above-mentioned challenges of Na metal anode. Due to its unique structure, the as-fabricated Na<sub>15</sub>Sn<sub>4</sub>/Na composite exhibited exceptional processability in contrast to the soft and sticky pure metallic Na, and can be easily fabricated into foils with small thickness (e.g., 100 μm). Na<sub>15</sub>Sn<sub>4</sub>/Na||Na<sub>15</sub>Sn<sub>4</sub>/Na symmetric cell exhibited stable electrochemical stripping/plating cycling for 100 cycles with constant overpotential of less than 15 mV at 1 mA cm<sup>-2</sup> and 1 mAh cm<sup>-2</sup> at 60°C. Even at harsh 90°C, the symmetric cell showed stable cycling with a low overpotential of around 3 mV at 1 mA cm<sup>-2</sup> and 1 mAh cm<sup>-2</sup>. Furthermore, Na<sub>0.9</sub>[Cu<sub>0.22</sub>Fe<sub>0.30</sub>Mn<sub>0.48</sub>]O<sub>2</sub> (NCFMO)||Na<sub>15</sub>Sn<sub>4</sub>/Na cell demonstrated high rate capability (98 mAh g<sup>-1</sup> at 2 C) and cyclability (88% capacity retention for 100 cycles) in comparison to the counterpart with pure Na metal anode (92 mAh g<sup>-1</sup> at 2 C, 80% capacity retention for 100 cycles). The concept of introducing metal alloy in sodium using cold calendaring to improve processability and electrochemical properties at elevated temperature can be expanded to other alkali metal electrodes in the future.

### Introduction

Due to their considerable energy density, abundance of Na resources, and potentially low cost, Na metal batteries are promising battery systems for various energy applications in modern society, such as electric vehicles and grid energy storage [1–6]. Recently, Na metal batteries with solid Na metal anode and liquid organic electrolyte have been widely investigated at room temperature [7–11]. However, poor processability of metallic Na requires complicated electrode fabrication technology, and high chemical reactivity lead to safety concerns, low Coulombic efficiency (CE) and inferior cycling stability [12–15]. Since the redox potential of metallic Na lies below the electrochemical window of liquid electrolyte, a solid electrolyte interphase (SEI) forms on the surface of metallic Na caused by the reaction between metallic Na and liquid

electrolyte [16–20]. The repeated large volume fluctuation during the plating/stripping of metallic Na inevitably destroys the formed SEI and causes the exposure of fresh surface of metallic Na to the electrolyte again, which subsequently consumes active Na and electrolyte to continuously generate new SEI. Furthermore, the parasitic reactions between Na metal and liquid electrolyte become more serious at elevated temperature (e.g., ≥ 60 °C), which is undesirable for batteries in outdoor energy storage devices and electric vehicles [21].

To achieve better Na metal electrode, various strategies have been explored, including the optimization of electrolyte, surface engineering, and the design of host materials (or current collectors) [22–30]. However, stable cycling of metallic Na electrode in carbonate electrolyte at elevated temperature (≥ 60 °C), which is important in practical battery application as mentioned above, remains a great challenge. As Na metal

\* Corresponding author.

E-mail address: [yongmingsun@hust.edu.cn](mailto:yongmingsun@hust.edu.cn) (Y. Sun).

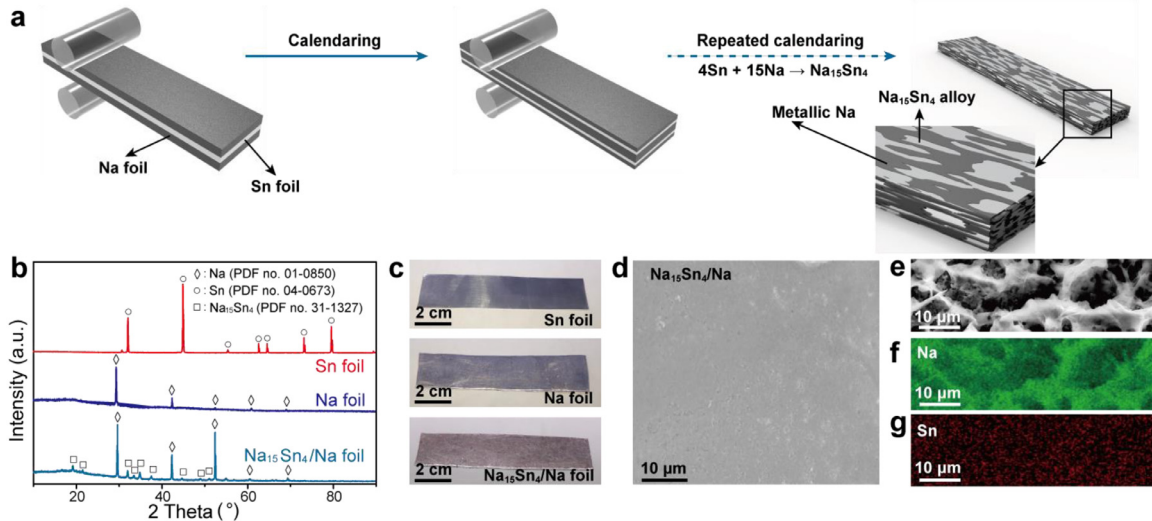


**Fig. 1.** Fabrication and characterizations of Na<sub>15</sub>Sn<sub>4</sub>/Na composite. (a) Schematic of the formation of Na<sub>15</sub>Sn<sub>4</sub>/Na composite foil. (b) XRD patterns of Sn foil, Na foil, and Na<sub>15</sub>Sn<sub>4</sub>/Na foil. (c) Optical images of Sn foil, Na foil, and Na<sub>15</sub>Sn<sub>4</sub>/Na composite foil. (d) SEM images of initial Na<sub>15</sub>Sn<sub>4</sub>/Na composite foil. (e) SEM image of Na<sub>15</sub>Sn<sub>4</sub>/Na composite after stripping 20 mAh cm<sup>-2</sup> of metallic Na at 1 mA cm<sup>-2</sup> (taken at 15 kV) and the corresponding EDS mapping images of Na element (f) and Sn (g) element, suggesting the uniform composite of Na<sub>15</sub>Sn<sub>4</sub> and Na.

is soft with a low melting point (98 °C), the increased working temperature not only enhances the side reactions between Na metal and electrolyte, but also causes serious safety concerns due to the collapse of the initial structure of pure Na metal electrode. Moreover, processing and molding of soft and sticky metallic Na are also challenging for its large-scale commercialization [31–33].

Herein, we fabricated a Na<sub>15</sub>Sn<sub>4</sub>/Na composite featuring uniform mixture of metallic Na and Na<sub>15</sub>Sn<sub>4</sub> network through a simple cold calendaring approach using metallic Na and Sn as the initial materials, where Na<sub>15</sub>Sn<sub>4</sub> is *in-situ* generated and implanted in Na metal matrix due to the spontaneous alloy reaction (4Sn + 15Na → Na<sub>15</sub>Sn<sub>4</sub>) during the repeated calendaring process (Fig. 1a). The Na<sub>15</sub>Sn<sub>4</sub>/Na composite shows much better processability than the pure metallic Na due to the enhanced mechanical property from alloying. In the Na<sub>15</sub>Sn<sub>4</sub>/Na composite, the Na<sub>15</sub>Sn<sub>4</sub> is stable in the working potential for plating and stripping of metallic Na due to its high desodiation potential (> 0.15 V vs. Na<sup>+</sup>/Na) [34]. It not only endows the electrode with uniform electron and Na<sup>+</sup> fluxes on the electrode to avoid the growth of dendrites, but also acts as a stable host to alleviate the problem of volume change, and thus maintain the integrity of the electrode and suppress the generation of thick SEI during the stripping/plating cycling of metallic Na. High ionic conductivity of the Na<sub>15</sub>Sn<sub>4</sub> matrix [35] enables rapid ion transport over the entire electrode and good rate capability. In contrast to bare metallic Na electrode or the metallic Na electrode with non-ionic conductive network, the electrode-electrolyte moves during the Na striping/plating cycles, leading to serious electrode corrosion, the stable structure without overall volume change of Na<sub>15</sub>Sn<sub>4</sub>/Na composite electrode enables a stable electrode interphase that excludes the electrolyte from within the electrode during cycling and, thus the SEI layer on the Na<sub>15</sub>Sn<sub>4</sub>/Na electrode is fixed in place on top of the electrode, which reduces the continuous growth of SEI or the consumption of electrolyte [36]. As expected, the as-fabricated Na<sub>15</sub>Sn<sub>4</sub>/Na electrode exhibited stable cycling with overpotential of 15 mV for 100 cycles in symmetric cells at 60 °C under 1 mA cm<sup>-2</sup> and 1 mAh cm<sup>-2</sup>. In contrast, short circuit took place after only 8 cycles for bare metallic Na under the same test condition. Moreover, good electrochemical stability was also achieved for the symmetric cell cycled at 90 °C. In addition, Na<sub>0.9</sub>[Cu<sub>0.22</sub>Fe<sub>0.30</sub>Mn<sub>0.48</sub>]O<sub>2</sub>(NCFMO)||Na<sub>15</sub>Sn<sub>4</sub>/Na cell demonstrated stable cycling at moderately high current density (98 mAh g<sup>-1</sup>, 2 C, 88% capacity retention after 100 cycles at 60 °C).

## Experimental

**Synthesis of Na<sub>15</sub>Sn<sub>4</sub>/Na** Sn foil was used as received (50 μm in thickness, 2.5 cm in width, Sinopharm Chemical). Metallic Na (Sinopharm Chemical) was pressed and cut into the same size as the Sn foil. During the fabrication, a Sn foil was sandwiched between two pieces of metallic Na with a molar of 11.25/1 for Na to Sn, and repeated calendaring and folding operation (15 times) was performed with a controlled calendaring gap (e.g., 400 μm) on a calendaring machine. All fabrication operations were conducted in an argon-filled glove box (<1 ppm H<sub>2</sub>O and O<sub>2</sub>).

**Material Characterizations** A Philips X' Pert diffractometer with Cu K $\alpha$  radiation ( $\lambda = 1.5418 \text{ \AA}$ ) was employed for identifying the phase information of the samples. Samples were sealed with Kapton tape to isolate from oxygen and moisture in the air in an argon-filled glove box before measurement. Scanning electron microscopy (SEM) and energy dispersive X-ray spectroscopy (EDS) mapping of samples were observed by a GeminiSEM300 field-emission scanning electron microscopy under an acceleration voltage of 5 kV and 15 kV, respectively. Samples were sealed in argon before their transfer to the SEM chamber. X-ray photoelectron spectra (XPS) measurements were conducted on an AXIS-ULTRA DLD spectrometer with Al K $\alpha$  radiation.

**Electrochemical Measurements** To investigating the electrochemical performance of the samples, a variety of cell configurations including Na<sub>15</sub>Sn<sub>4</sub>/Na||Na<sub>15</sub>Sn<sub>4</sub>/Na, Na||Na, [Cu<sub>0.22</sub>Fe<sub>0.30</sub>Mn<sub>0.48</sub>]O<sub>2</sub>(NCFMO)||Na<sub>15</sub>Sn<sub>4</sub>/Na, and Na<sub>0.9</sub>[Cu<sub>0.22</sub>Fe<sub>0.30</sub>Mn<sub>0.48</sub>]O<sub>2</sub>||Na cells were fabricated with coin cell configuration (CR2025) in an argon-filled glove box, using 1 M NaClO<sub>4</sub> in ethylene carbonate/propylene carbonate (EC/PC, 1:1, volume ratio) with 5 wt% fluoroethylene carbonate (FEC) as the electrolyte and glass fiber membrane as the separator. The NCFMO electrodes were prepared via a slurry method by mixing the NCFMO powder (80 wt%), Super P (10 wt%), and polyvinylidene fluoride (PVDF, 10 wt%) in *N*-methyl pyrrolidone (NMP) and casting the slurry onto an Al foil. Galvanostatic charge/discharge measurements of cells were conducted on Neware multi-channel battery testing instruments. Electrochemical impedance spectroscopy (EIS) was performed on a Biologic VMP3 electrochemistry workstation with the frequency range between 10 mHz and 100 kHz.

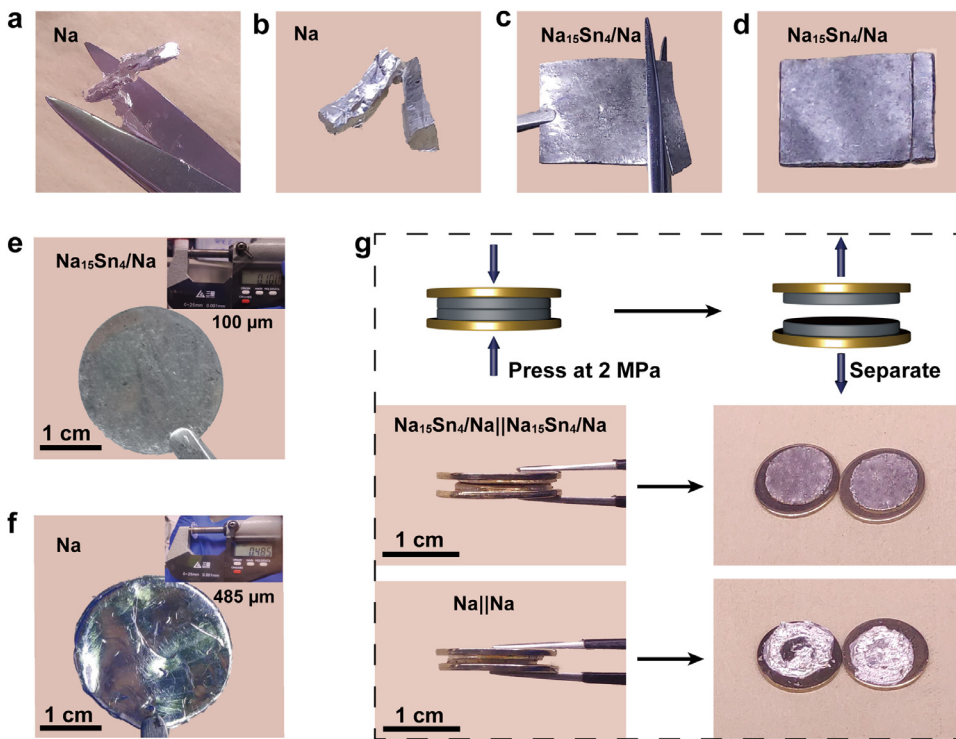


**Fig. 2.** The comparison of processability between Na<sub>15</sub>Sn<sub>4</sub>/Na and bare Na. (a, b) Digital camera images of Na during tailing (a) and after tailing apart (b). (c, d) Digital camera images of as-fabricated Na<sub>15</sub>Sn<sub>4</sub>/Na foil during tailing (c) and after tailing into designed geometric shapes (d). (e, f) Digital camera images of as-fabricated Na<sub>15</sub>Sn<sub>4</sub>/Na foil (e) and Na flake (f) after compressing to a certain thickness. (g) Schematic illustration and optical images of Na<sub>15</sub>Sn<sub>4</sub>/Na and Na foils under external loading and release.

## Results and discussion

Due to the good ductility of metallic Na and Sn [37], a Na|Sn|Na sandwich consisting of two metallic Na foils and one Sn foil can be repeatedly calendered without fracture (Fig. 1a). Metallic Na is very soft and sticky, and is easy to be adhered closely to metallic Sn during the mechanical calendering processing of the Na|Sn|Na sandwich. After repeated cycling of mechanical calendering, a uniform composite foil (90 × 20 mm) is fabricated and stable interface between metallic Sn and Na is created within the composite (Fig. 1a and c). Moreover, the enthalpy change ( $\Delta H$ ) for the reaction 4Sn + 15Na → Na<sub>15</sub>Sn<sub>4</sub> is -296 kJ mol<sup>-1</sup> at 298K, indicating that alloy reaction between metallic Na and metallic Sn can take place spontaneously [34,38–40]. X-ray diffraction (XRD) was conducted to identify the compositional evolution of Na<sub>15</sub>Sn<sub>4</sub>/Na composite (Fig. 1b). The disappearance of the diffraction peaks for metallic Sn indicated the alloy reaction between metallic Sn and metallic Na, and the XRD pattern of Na<sub>15</sub>Sn<sub>4</sub>/Na foil further verified that metallic Sn was converted to Na<sub>15</sub>Sn<sub>4</sub>. Meanwhile, strong diffraction peaks of metallic Na in the XRD pattern of Na<sub>15</sub>Sn<sub>4</sub>/Na composite were still observed due to the stoichiometric excess of metallic Na. The as-achieved Na<sub>15</sub>Sn<sub>4</sub>/Na composite showed a foil structure, similar to the pristine Sn foil (Fig. 1c). Smooth surface was observed under scanning electron microscopy (SEM, Fig. 1d). After stripping 20 mAh cm<sup>-2</sup> of metallic Na at 1 mA cm<sup>-2</sup> for a thin Na<sub>15</sub>Sn<sub>4</sub>/Na composite electrode, a cross-linked Na<sub>15</sub>Sn<sub>4</sub> network was observed from energy dispersive X-ray spectroscopy (EDS) mapping images of Na and Sn elements (Fig. 1e, f, and g), suggesting the uniform distribution of Na<sub>15</sub>Sn<sub>4</sub> in the composite. Such 3D Na<sub>15</sub>Sn<sub>4</sub> can provide the stable framework for buffering the volume change and maintaining the structural integrity during Na stripping/plating cycling, and offer the pathway for sodium ion transport within the entire Na<sub>15</sub>Sn<sub>4</sub>/Na composite electrode, which can improve the electrochemical sodium storage properties.

The processability of metallic Na and Na<sub>15</sub>Sn<sub>4</sub>/Na composite was further investigated. Due to the soft and sticky nature, metallic Na could not form a stable geometric shape by regular shearing (Fig. 2a and b). In addition, metallic Na could deform easily under external pressure, leading to the uneven and almost crimped surface of bare Na foil even at

large thickness of 485 μm (Fig. 2f). Such inferior processing properties hinder the application of bare metallic Na electrode in battery industry. In contrast, the processability of the as-fabricated Na<sub>15</sub>Sn<sub>4</sub>/Na composite was much improved, which was demonstrated by the easy tailoring of the as-fabricated Na<sub>15</sub>Sn<sub>4</sub>/Na composite foil to designed geometric shapes (Fig. 2c and d) and the successful generation of thin foil with the thickness of 100 μm by a simple calendering process (Fig. 2e). Furthermore, under external loading of 2 MPa (Figure S1), two metallic Na disks adhered together while two Na<sub>15</sub>Sn<sub>4</sub>/Na composite foils remained separate after release (Fig. 2g). Therefore, the processability of the Na<sub>15</sub>Sn<sub>4</sub>/Na composite is much improved in comparison to the bare metallic Na, making it feasible in the application in battery industry or other fields. This may be attributed to the uniformly distributed Na<sub>15</sub>Sn<sub>4</sub> in the composite, which can greatly increase the hardness and improve the mechanical property of Na<sub>15</sub>Sn<sub>4</sub>/Na composite, thus enhancing its moldability and processability.

To evaluate the electrochemical properties of Na<sub>15</sub>Sn<sub>4</sub>/Na electrode, Na<sub>15</sub>Sn<sub>4</sub>/Na||Na<sub>15</sub>Sn<sub>4</sub>/Na symmetric cells were fabricated. Carbonate-based electrolytes are widely used in battery industry due to their wide electrochemical window in comparison to ether-based electrolytes [41,42]. However, the application of a carbonate-based electrolyte is challenging for metal electrodes (e.g., Li metal and Na metal) due to its fragile SEI structure [14,43,44]. During practical application, there exists undesirable situations where the batteries are operated at elevated temperature (e.g., ≥ 60 °C), especially for electric vehicles and outdoor energy storage devices. However, due to the high reactivity of metallic Na, it is challenging to achieve good electrochemical property of Na metal electrodes at elevated temperature. Previous study revealed that Na||Na symmetric cells could only endure few cycles at 60 °C in an electrolyte consisting of 1 M NaClO<sub>4</sub> in EC/DEC with 5 wt% FEC due to the severe side reactions between metallic Na and electrolyte [21]. To show the advancement of Na<sub>15</sub>Sn<sub>4</sub>/Na electrode with high electrochemical stability and chemical stability at elevated temperature, galvanostatic cycling tests of Na<sub>15</sub>Sn<sub>4</sub>/Na||Na<sub>15</sub>Sn<sub>4</sub>/Na symmetric cells were conducted at 60 °C with the same electrolyte. Voltage profiles of Na<sub>15</sub>Sn<sub>4</sub>/Na||Na<sub>15</sub>Sn<sub>4</sub>/Na and Na||Na symmetric cells were compared at various current densities of 1, 3, and 5 mA cm<sup>-2</sup> with areal capacity

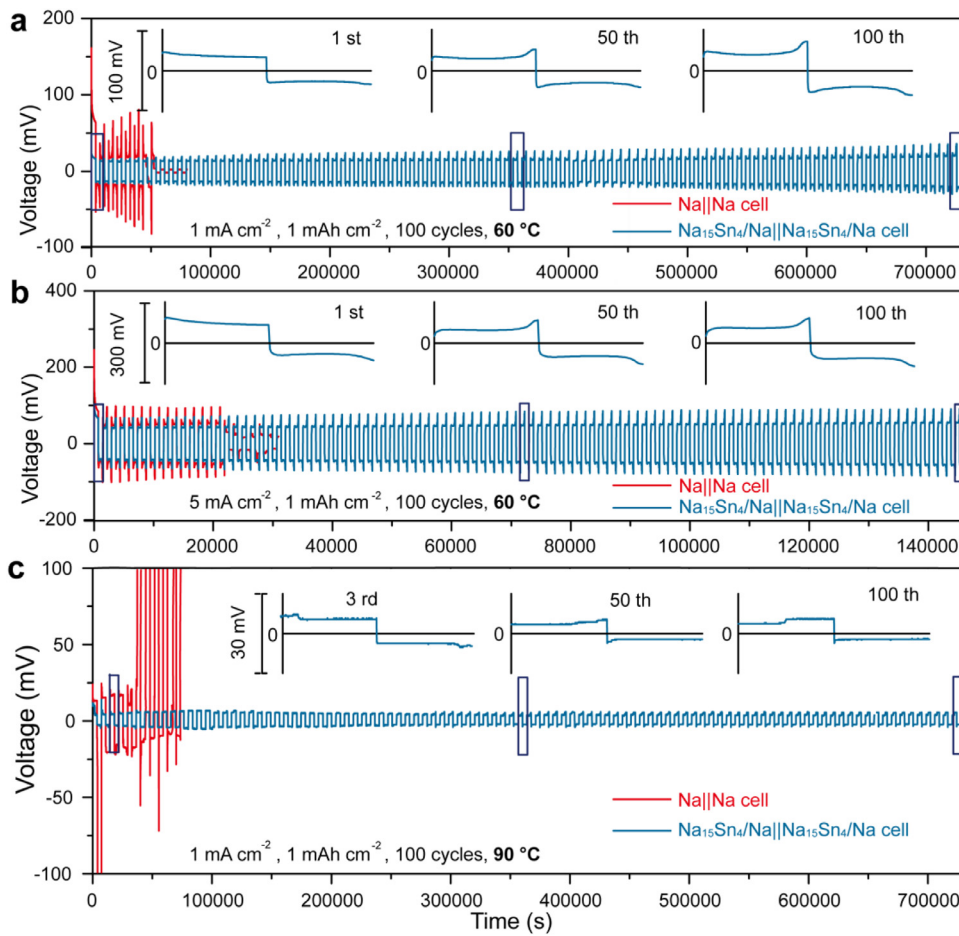


**Fig. 3.** Electrochemical performance of  $\text{Na}_{15}\text{Sn}_4/\text{Na}||\text{Na}_{15}\text{Sn}_4/\text{Na}$  and  $\text{Na}||\text{Na}$  symmetric cells at elevated temperature. (a, b) Galvanostatic cycling of  $\text{Na}_{15}\text{Sn}_4/\text{Na}||\text{Na}_{15}\text{Sn}_4/\text{Na}$  and  $\text{Na}||\text{Na}$  symmetric cells under current density of  $1 \text{ mA cm}^{-2}$  (a) and  $5 \text{ mA cm}^{-2}$  (b) with the capacity fixed at  $1 \text{ mAh cm}^{-2}$  at  $60^\circ\text{C}$ . (c) Galvanostatic cycling of  $\text{Na}_{15}\text{Sn}_4/\text{Na}||\text{Na}_{15}\text{Sn}_4/\text{Na}$  and  $\text{Na}||\text{Na}$  cells under current density of  $1 \text{ mA cm}^{-2}$  with the capacity fixed at  $1 \text{ mAh cm}^{-2}$  at  $90^\circ\text{C}$ .

fixed at  $1 \text{ mAh cm}^{-2}$  (Fig. 3a, b and S2).  $\text{Na}_{15}\text{Sn}_4/\text{Na}$  electrode showed stable voltage profiles for 100 cycles with small overpotential of  $< 15 \text{ mV}$  at  $1 \text{ mA cm}^{-2}$ , whereas bare Na metal electrode demonstrated much larger overpotential ( $> 50 \text{ mV}$ ) with large voltage fluctuation during cycling. The  $\text{Na}||\text{Na}$  symmetric cell quickly failed after only 8 cycles (Fig. 3a). When cycled at higher current densities ( $3 \text{ mA cm}^{-2}$  and  $5 \text{ mA cm}^{-2}$ ),  $\text{Na}_{15}\text{Sn}_4/\text{Na}$  electrode displayed stable voltage-time plots during the measured cycles (200 hours), in sharp contrast to fast cell short circuit of the bare Na metal electrode within 32 hours (Fig. 3b and S2). The overpotential of the  $\text{Na}_{15}\text{Sn}_4/\text{Na}$  electrode at  $5 \text{ mA cm}^{-2}$  was only  $50 \text{ mV}$ , which ranked among the best metallic Na electrode [29,31,45,46]. We further raised the test temperature to  $90^\circ\text{C}$ , close to the melting point of bare Na (Figure S3), and the  $\text{Na}_{15}\text{Sn}_4/\text{Na}||\text{Na}_{15}\text{Sn}_4/\text{Na}$  symmetric cell still demonstrated stable cycling for 200 hours with smooth potential and low overpotential ( $< 5 \text{ mV}$  at  $1 \text{ mA cm}^{-2}$ ) after the activation cycles (Fig. 3c), while  $\text{Na}||\text{Na}$  cell displayed large fluctuations and short circuited after 20 cycles. We also conducted the electrochemical cycling of  $\text{Na}_{15}\text{Sn}_4/\text{Na}||\text{Na}_{15}\text{Sn}_4/\text{Na}$  and  $\text{Na}||\text{Na}$  symmetric cells at room temperature ( $25^\circ\text{C}$ , Figure S4a and b). Significant improvement of the  $\text{Na}_{15}\text{Sn}_4/\text{Na}$  electrode was also observed, featuring much more stable cycling and much lower overpotential under the test condition ( $1$  and  $2 \text{ mA cm}^{-2}$ ,  $1 \text{ mAh cm}^{-2}$ ) in comparison to the bare  $\text{Na}||\text{Na}$  symmetric cells and most of recently reported data (Table S1). Electrochemical impedance spectroscopy (EIS) was conducted for the  $\text{Na}_{15}\text{Sn}_4/\text{Na}$  and bare Na electrodes before and after cycling at  $60^\circ\text{C}$  (Figure S5). The  $\text{Na}_{15}\text{Sn}_4/\text{Na}$  showed a much lower interfacial resistance of  $75 \Omega$  after 10 cycles in comparison to  $150 \Omega$  for the bare Na, which verified the significant role of  $\text{Na}_{15}\text{Sn}_4/\text{Na}$  composite structure in suppressing the side reactions between the electrolyte and metallic Na and improving the electrochemical performance. The failure mech-

anisms are different for the  $\text{Na}||\text{Na}$  cells after cycling at various temperature in carbonate electrolyte. As verified by EIS results in Figure S6,  $\text{Na}||\text{Na}$  cells failed at  $60^\circ\text{C}$  featured by short circuit, probably due to the accumulation of metallic Na dendrites. In contrast, the failure of the  $\text{Na}||\text{Na}$  cell cycled at  $90^\circ\text{C}$  was mainly caused by the severe parasitic corrosion between the electrolyte and electrode, as evidenced by the significantly increased resistance after cycling (100+ times higher).

Due to lower melting point and high chemical reactivity, Na is susceptible to high temperature in organic liquid electrolyte systems. The chemical stability of symmetric cells fabricated respectively with bare Na and  $\text{Na}_{15}\text{Sn}_4/\text{Na}$  electrodes at elevated temperature was also evaluated by EIS. The measurements were conducted at  $60^\circ\text{C}$  for symmetric cells after preserving at  $60^\circ\text{C}$  for different time periods (Figure S7a and b). With preserving time prolonged from 24 to 120 h, the increase in value and the absolute value of the resistance in high-frequency range for  $\text{Na}_{15}\text{Sn}_4/\text{Na}$  electrode were much smaller than that of the bare Na. Additionally, an emerging semicircle located at middle frequency range was observed, which might be ascribed to the accumulation of non-conductive by-product due to parasite reactions between metal anode and the electrolyte [22]. The corresponding resistance change for  $\text{Na}_{15}\text{Sn}_4/\text{Na}$  electrode was negligible in comparison to that of the bare metallic Na electrode. The resistance for bare Na electrode increased to about  $4500 \Omega$  after preserving for 24 h, and kept at  $2500 \Omega$  after preserving for 120 h. These results indicated the much-improved chemical stability of  $\text{Na}_{15}\text{Sn}_4/\text{Na}$  electrode at elevated temperature. Here, we emphasize that the parasitic corrosion reactions at  $60^\circ\text{C}$  were much more drastic than at  $25^\circ\text{C}$  for active Na metal. Thus, the  $\text{Na}_{15}\text{Sn}_4/\text{Na}$  electrode had much better anticorrosive property to the electrolyte than the bare Na metal electrode.

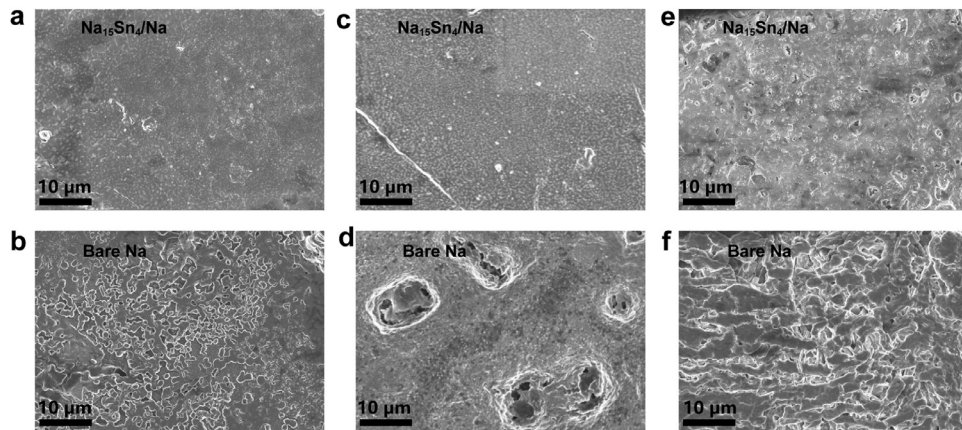


**Fig. 4.** Electrochemical Na stripping and plating behavior of Na<sub>15</sub>Sn<sub>4</sub>/Na and bare Na electrodes. (a, b, c, d) Top-view SEM images of Na<sub>15</sub>Sn<sub>4</sub>/Na and bare Na electrodes after electrochemical (a, b) plating and (c, d) stripping of metallic Na (0.25 mA cm<sup>-2</sup>, 0.25 mAh cm<sup>-2</sup>). (e, f) Top-view SEM images of Na<sub>15</sub>Sn<sub>4</sub>/Na (e) and bare Na metal (f) electrodes after a full galvanostatic plating/stripping cycle at 0.5 mA cm<sup>-2</sup> and 0.5 mAh cm<sup>-2</sup>.

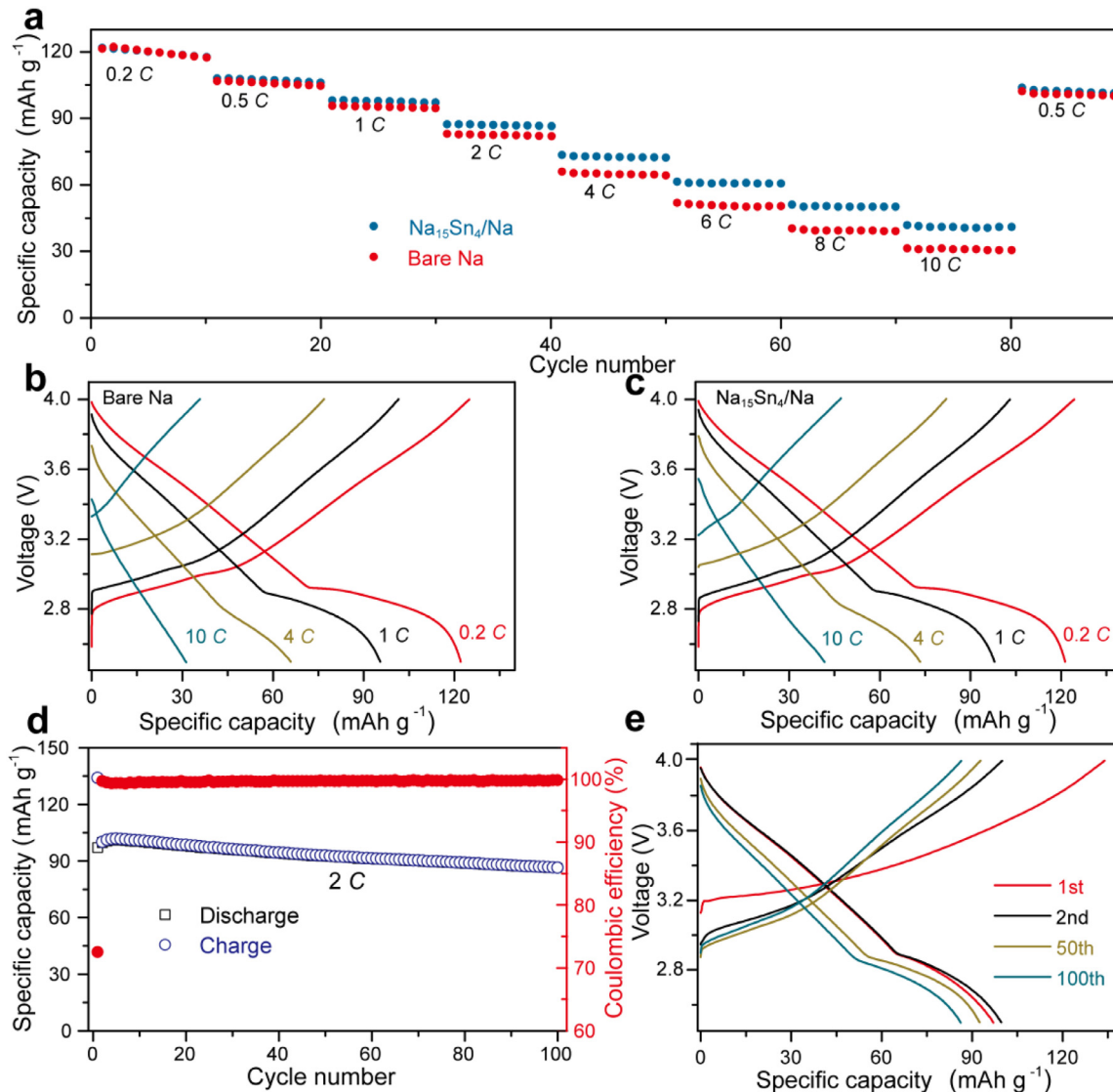


**Fig. 5.** Electrochemical performance of NCFMO||Na<sub>15</sub>Sn<sub>4</sub>/Na and NCFMO||Na cells at 60°C. (a) Rate capability of NCFMO||Na<sub>15</sub>Sn<sub>4</sub>/Na cell and NCFMO||Na cell at various rates from 0.2 to 10 C, (1 C = 150 mA g<sup>-1</sup>). (b, c) Voltage profile comparison of NCFMO||Na<sub>15</sub>Sn<sub>4</sub>/Na cell (b) and NCFMO||Na cell (c) at various rates. (d, e) Cyclability of NCFMO||Na<sub>15</sub>Sn<sub>4</sub>/Na cell at 2 C (d) and galvanostatic charge/discharge curves for different cycles (e).

To further explain the good electrochemical property of  $\text{Na}_{15}\text{Sn}_4/\text{Na}$  electrode, Na stripping/plating morphology of the  $\text{Na}_{15}\text{Sn}_4/\text{Na}$  composite was examined. After electrochemical plating of metallic Na ( $0.25 \text{ mAh cm}^{-2}$ ,  $0.25 \text{ mA cm}^{-2}$ ), the  $\text{Na}_{15}\text{Sn}_4/\text{Na}$  electrode showed a smooth surface (Fig. 4a), indicating uniform Na plating behavior. In contrast, uneven mossy Na structures were observed on the bare metallic Na electrode (Fig. 4b). The surface of the  $\text{Na}_{15}\text{Sn}_4/\text{Na}$  electrode remained smooth and flat after electrochemical Na stripping of  $0.25 \text{ mAh cm}^{-2}$  at  $0.25 \text{ mA cm}^{-2}$  (Fig. 4c), suggesting uniform electrochemical stripping behavior. In contrast, numerous randomly distributed voids with size of several micrometers were observed in the top-view SEM image of the bare Na metal electrode (Fig. 4d). After plating  $2 \text{ mAh cm}^{-2}$  of metallic Na on a  $\text{Na}_{15}\text{Sn}_4/\text{Na}$  electrode at  $0.2 \text{ mA cm}^{-2}$ , a dense and uniform plating layer was observed and the thickness was  $\sim 20 \mu\text{m}$ . In contrast, bare Na electrode shows loose and porous surface plating layer with much large thickness ( $\sim 35 \mu\text{m}$ ) under the same plating condition (Figure S8). Uniform stripping and plating behavior of metallic Na for the  $\text{Na}_{15}\text{Sn}_4/\text{Na}$  electrode was further evidenced by the SEM results of the electrode after a full electrochemical stripping/plating cycle, and the  $\text{Na}_{15}\text{Sn}_4/\text{Na}$  electrode demonstrated a more compact and smoother surface structure than the bare Na metal electrode (Fig. 4e and f). After 10 cycles at  $1 \text{ mAh cm}^{-2}$  and  $1 \text{ mA cm}^{-2}$ , a porous and loose interphase layer with the thickness of  $\sim 40 \mu\text{m}$  was observed for bare Na electrode, while  $\text{Na}_{15}\text{Sn}_4/\text{Na}$  electrode preserved its uniform and dense structure (Figure S10). The  $\text{Na}_{15}\text{Sn}_4$  framework provides abundant pathways for charge transfer over the whole electrode [36], which greatly mitigates the localized non-uniform deposition and dissolution of metallic Na. Therefore, the inherent inhomogeneous electrochemical deposition/dissolution behavior of metallic Na has been suppressed by the composite structural design of  $\text{Na}_{15}\text{Sn}_4/\text{Na}$  electrode.

To validate the feasibility of as-designed  $\text{Na}_{15}\text{Sn}_4/\text{Na}$  anode for sodium metal batteries, we compared the electrochemical performance of cells using  $\text{Na}_{15}\text{Sn}_4/\text{Na}$  or bare Na anode paired with a NCFMO cathode. The active mass loading of NCFMO powder was  $\sim 6.5 \text{ mg cm}^{-2}$ . As expected, NCFMO|| $\text{Na}_{15}\text{Sn}_4/\text{Na}$  cell outperformed NCFMO||Na cell in terms of rate capability, particularly at high rates (Fig. 5a). The reversible capacities of NCFMO|| $\text{Na}_{15}\text{Sn}_4/\text{Na}$  cell reached 61 (52% of the capacity at  $0.2 \text{ C}$ ), 50, and  $41 \text{ mAh g}^{-1}$  at the high rates of 6, 8, and  $10 \text{ C}$ , respectively, higher than 50, 39, and  $30 \text{ mAh g}^{-1}$  for the NCFMO||Na cell. The much enhanced rate capability at high current densities arise from the high conductivity of the  $\text{Na}_{15}\text{Sn}_4$  framework. Meanwhile, reduced potential hysteresis and lower overpotential of each charging plateau at various rates were observed for NCFMO|| $\text{Na}_{15}\text{Sn}_4/\text{Na}$  cell, indicating enhanced kinetics of  $\text{Na}_{15}\text{Sn}_4/\text{Na}$  anode in comparison to bare Na anode (Fig. 5b and c). The NCFMO|| $\text{Na}_{15}\text{Sn}_4/\text{Na}$  cell also exhibited more stable cycling than the NCFMO||Na cell under high current density of  $2 \text{ C}$  (Fig. 5d and Figure S11). Even after 100 charge/discharge cycles, the reversible capacity remained at  $86 \text{ mAh g}^{-1}$  (88% of the initial value) and still maintained characteristic Na deintercalation/intercalation electrochemical process of NCFMO material (Fig. 5e) [47,48]. Moreover, the NCFMO|| $\text{Na}_{15}\text{Sn}_4/\text{Na}$  cell still demonstrated good cyclability and rate capability at room temperature ( $25^\circ\text{C}$ ), which are much better than that of the counterpart using bare Na anode (Figure S12). The remarkably improved electrochemical performance of  $\text{Na}_{15}\text{Sn}_4/\text{Na}$  anode further verifies its potential for advancement of  $\text{Na}_{15}\text{Sn}_4/\text{Na}$  for rechargeable Na metal batteries.

## Conclusions

In summary, a mechanically robust  $\text{Na}_{15}\text{Sn}_4/\text{Na}$  composite with high electrochemical anticorrosivity was fabricated through a simple cold calendaring method. The *in-situ* formed  $\text{Na}_{15}\text{Sn}_4$  alloy was homogeneously implanted in the Na metal, enabling the composite with much enhanced moldability and processability. The introduction of  $\text{Na}_{15}\text{Sn}_4$  effectively regulated the Na dissolution/deposition behavior, and thus inhibited the Na dendrite growth. Symmetrical cells with resultant

$\text{Na}_{15}\text{Sn}_4/\text{Na}$  electrodes demonstrated low voltage overpotential and impressive cycle stability even at  $60$  and  $90^\circ\text{C}$ , due to the much more improved chemical and electrochemical stability against elevated temperature in comparison to the bare Na metal electrode. NCFMO|| $\text{Na}_{15}\text{Sn}_4/\text{Na}$  cells show excellent rate performance and stable cycling at a high current density of  $2 \text{ C}$ . Considering the outstanding mechanical processability and electrochemical properties and the facile fabrication, we believe the utilization of  $\text{Na}_{15}\text{Sn}_4/\text{Na}$  composite will accelerate the development of Na metal and other next-generation batteries.

## Notes

The authors declare no competing financial interest.

## Declaration of Competing Interest

The authors declare no competing financial interest.

## Acknowledgements

Y.S. acknowledges the support from the [Natural Science Foundation of China](#) (grant no. [52072137](#), [51802105](#)) and the financial support by the Innovation Fund of Wuhan National Laboratory for Optoelectronics of Huazhong University of Science and Technology. X.L. acknowledges the support from the [Natural Science Foundation of China](#) (grant no. [52002136](#)). Z.W.S acknowledges the support of the [Singapore National Research Foundation](#) ([NRF-NRFF2017-04](#)). The authors would like to thank the Analytical and Testing Center of Huazhong University of Science and Technology as well as the Center for Nanoscale Characterization & Devices of Wuhan National Laboratory for Optoelectronics for providing the facilities to conduct the characterization.

## Supplementary materials

Supplementary material associated with this article can be found, in the online version, at doi:[10.1016/j.ensm.2020.11.015](https://doi.org/10.1016/j.ensm.2020.11.015).

## References

- [1] C.X. Zu, H. Li, Thermodynamic analysis on energy densities of batteries, *Energy Environ. Sci.* 4 (2011) 2614–2624.
- [2] J.Y. Hwang, S.T. Myung, Y.K. Sun, Sodium-ion batteries: present and future, *Chem. Soc. Rev.* 46 (2017) 3529–3614.
- [3] Y.S. Hong, N. Li, H. Chen, P. Wang, W.L. Song, D. Fang, In operando observation of chemical and mechanical stability of Li and Na dendrites under quasi-zero electrochemical field, *Energy Storage Mater* 11 (2018) 118–126.
- [4] P. Hartmann, C.L. Bender, M. Vračar, A.K. Dürr, A. Garsuch, J. Janek, P. Adelhelm, A rechargeable room-temperature sodium superoxide ( $\text{NaO}_2$ ) battery, *Nat. Mater.* 12 (2013) 228–232.
- [5] K.B. Hueso, M. Armand, T. Rojo, High temperature sodium batteries: status, challenges and future trends, *Energy Environ. Sci.* 6 (2013) 734–749.
- [6] X. Lu, G. Xia, J.P. Lemmon, Z. Yang, Advanced materials for sodium-beta alumina batteries: Status, challenges and perspectives, *J. Power Sources* 195 (2010) 2431–2442.
- [7] S. Wei, S. Xu, A. Agrawral, S. Choudhury, Y. Lu, Z. Tu, L. Ma, L.A. Archer, A stable room-temperature sodium-sulfur battery, *Nat. Commun.* 7 (2016) 11722.
- [8] R. Cao, K. Mishra, X. Li, J. Qian, M.H. Engelhard, M.E. Bowden, K.S. Han, K.T. Mueller, W.A. Henderson, J.G. Zhang, Enabling room temperature sodium metal batteries, *Nano Energy* 30 (2016) 825–830.
- [9] Z.W. Seh, J. Sun, Y. Sun, Y. Cui, A highly reversible room-temperature sodium metal anode, *ACS Cent. Sci.* 1 (2015) 449–455.
- [10] Y. Zhao, K.R. Adair, X. Sun, Recent developments and insights into the understanding of Na metal anodes for Na-metal batteries, *Energy Environ. Sci.* 11 (2018) 2673–2695.
- [11] L. Zeng, Y. Yao, J. Shi, Y. Jiang, W. Li, L. Gu, Y. Yu, A flexible  $S1-xSex@$ porous carbon nanofibers ( $x \leq 0.1$ ) thin film with high performance for Li-S batteries and room-temperature Na-S batteries, *Energy Storage Mater* 5 (2016) 50–57.
- [12] D. Lin, Y. Liu, Y. Cui, Reviving the lithium metal anode for high-energy batteries, *Nat. Nanotech.* 12 (2017) 194–206.
- [13] P. Albertus, S. Babinec, S. Litelman, A. Newman, Status and challenges in enabling the lithium metal electrode for high-energy and low-cost rechargeable batteries, *Nat. Energy* 3 (2017) 16–21.
- [14] B. Lee, E. Paek, D. Mitlin, S.W. Lee, Sodium metal anodes: emerging solutions to dendrite growth, *Chem. Rev.* 119 (2019) 5416–5460.

- [15] L. Fu, C. Shang, J. Ma, C. Zhang, X. Zang, J. Chai, J. Li, G. Cui, Cu<sub>2</sub>GeS<sub>3</sub> derived ultrafine nanoparticles as high-performance anode for sodium ion battery, *Sci. China Mater.* 61 (2018) 1177–1184.
- [16] H. Kim, G. Jeong, Y.U. Kim, J.H. Kim, C.M. Park, H.-J. Sohn, Metallic anodes for next generation secondary batteries, *Chem. Soc. Rev.* 42 (2013) 9011–9034.
- [17] E. Peled, S. Menkin, Review-SEI: past, present and future, *J. Electrochem. Soc.* 164 (2017) A1703–A1719.
- [18] C. Zhao, Y. Lu, J. Yue, D. Pan, Y. Qi, Y. Hu, L. Chen, Advanced Na metal anodes, *J. Energy Chem.* 27 (2018) 1584–1596.
- [19] J. Wang, Y. Yamada, K. Sodeyama, E. Watanabe, K. Takada, Y. Tateyama, A. Yamada, Fire-extinguishing organic electrolytes for safe batteries, *Nat. Energy* 3 (2018) 22–29.
- [20] X. Zheng, Z. Gu, X. Liu, Z. Wang, J. Wen, X. Wu, W. Luo, Y. Huang, Bridging the immiscibility of an all-fluoride fire extinguishant with highly-fluorinated electrolytes toward safe sodium metal batteries, *Energy Environ. Sci.* 13 (2020) 1788–1798.
- [21] D. Lei, Y. He, H. Huang, Y. Yuan, G. Zhong, Q. Zhao, X. Hao, D. Zhang, C. Lai, S. Zhang, J. Ma, Y. Wei, Q. Yu, W. Lv, Y. Yu, B. Li, Q. Yang, Y. Yang, J. Lu, F. Kang, Cross-linked beta alumina nanowires with compact gel polymer electrolyte coating for ultra-stable sodium metal battery, *Nat. Commun.* 10 (2019) 4244.
- [22] Z. Xu, J. Yang, T. Zhang, L. Sun, Y. Nuli, J. Wang, S.i. Hirano, Stable Na metal anode enabled by a reinforced multistructural SEI layer, *Adv. Funct. Mater.* 29 (2019) 1901924.
- [23] J. Lee, Y. Lee, J. Lee, S.M. Lee, J.H. Choi, H. Kim, M.S. Kwon, K. Kang, K.T. Lee, N.S. Choi, Ultraconcentrated sodium bis(fluorosulfonyl)imide-based electrolytes for high-performance sodium metal batteries, *ACS Appl. Mater. Interfaces* 9 (2017) 3723–3732.
- [24] J. Zheng, S. Chen, W. Zhao, J. Song, M.H. Engelhard, J.G. Zhang, Extremely stable sodium metal batteries enabled by localized high-concentration electrolytes, *ACS Energy Lett.* 3 (2018) 315–321.
- [25] S. Liu, S. Tang, X. Zhang, A. Wang, Q.H. Yang, J. Luo, Porous Al current collector for dendrite-free Na metal anodes, *Nano Lett.* 17 (2017) 5862–5868.
- [26] W. Luo, Y. Zhang, S. Xu, J. Dai, E. Hitz, Y. Li, C. Yang, C. Chen, B. Liu, L. Hu, Encapsulation of metallic Na in an electrically conductive host with porous channels as a highly stable Na metal anode, *Nano Lett.* 17 (2017) 3792–3797.
- [27] Z. Hou, W. Wang, Y. Yu, X. Zhao, Q. Chen, L. Zhao, Q. Di, H. Ju, Z. Quan, Poly(vinylidene difluoride) coating on Cu current collector for high-performance Na metal anode, *Energy Storage Mater.* 24 (2020) 588–593.
- [28] T. Wang, Y. Liu, Y. Lu, Y. Hu, L. Fan, Dendrite-free Na metal plating/stripping onto 3D porous Cu hosts, *Energy Storage Mater.* 15 (2018) 274–281.
- [29] F. Wu, J. Zhou, R. Luo, Y. Huang, Y. Mei, M. Xie, R. Chen, Reduced graphene oxide aerogel as stable host for dendrite-free sodium metal anode, *Energy Storage Mater.* 22 (2019) 376–383.
- [30] L. Fu, C. Shang, G. Li, L. Hu, X. Zhang, L. Huang, X. Wang, G. Zhou, Lithium pre-cycling induced fast kinetics of commercial Sb<sub>2</sub>S<sub>3</sub> anode for advanced sodium storage, *Energy Environ. Sci.* 2 (2019) 209–215.
- [31] S. Chi, X. Qi, Y. Hu, L. Fan, 3D flexible carbon felt host for highly stable sodium metal anodes, *Adv. Energy Mater.* 8 (2018) 1702764.
- [32] A. Wang, X. Hu, H. Tang, C. Zhang, S. Liu, Y.W. Yang, Q.H. Yang, J. Luo, Processable and moldable sodium-metal anodes, *Angew. Chem., Int. Ed.* 56 (2017) 11921–11926.
- [33] C. Chu, N. Wang, L. Li, L. Lin, F. Tian, Y. Li, J. Yang, S.X. Dou, Y. Qian, Uniform nucleation of sodium in 3D carbon nanotube framework via oxygen doping for long-life and efficient Na metal anodes, *Energy Storage Mater.* 23 (2019) 137–143.
- [34] Z. Li, J. Ding, D. Mitlin, Tin and tin compounds for sodium ion battery anodes: phase transformations and performance, *Acc. Chem. Res.* 48 (2015) 1657–1665.
- [35] Z. Tu, S. Choudhury, M.J. Zachman, S. Wei, K. Zhang, L.F. Kourkoutis, L.A. Archer, Fast ion transport at solid-solid interfaces in hybrid battery anodes, *Nat. Energy* 3 (2018) 310–316.
- [36] M. Wan, S. Kang, L. Wang, H.W. Lee, G.W. Zheng, Y. Cui, Y. Sun, Mechanical rolling formation of interpenetrated lithium metal/lithium tin alloy foil for ultrahigh-rate battery anode, *Nat. Commun.* 11 (2020) 829.
- [37] H. Liu, H. Tang, M. Fang, W. Si, Q. Zhang, Z. Huang, L. Gu, W. Pan, J. Yao, C. Nan, H. Wu, 2D metals by repeated size reduction, *Adv. Mater.* 28 (2016) 8170–8176.
- [38] A. Jain, G. Hautier, S.P. Ong, C.J. Moore, C.C. Fischer, K.A. Persson, G. Ceder, Formation enthalpies by mixing GGA and GGA + U calculations, *Phys. Rev. B* 84 (2011) 045115.
- [39] V. Kumar, A.Y.S. Eng, Y. Wang, D.T. Nguyen, M.F. Ng, Z.W. Seh, An artificial metal-alloy interphase for high-rate and long-life sodium-sulfur batteries, *Energy Storage Mater.* 29 (2020) 1–8.
- [40] X. Zheng, H. Fu, C. Hu, H. Xu, Y. Huang, J. Wen, H. Sun, W. Luo, Y. Huang, Toward a stable sodium metal anode in carbonate electrolyte: a compact, inorganic alloy interface, *J. Phys. Chem. Lett.* 10 (2019) 707–714.
- [41] A. Ponrouch, E. Marchante, M. Courty, J.M. Tarascon, M.R. Palacín, In search of an optimized electrolyte for Na-ion batteries, *Energy Environ. Sci.* 5 (2012) 8572–8583.
- [42] K. Xu, Nonaqueous liquid electrolytes for lithium-based rechargeable batteries, *Chem. Rev.* 104 (2004) 4303–4418.
- [43] D. Zhang, A. Dai, M. Wu, K. Shen, T. Xiao, G. Hou, J. Lu, Y. Tang, Lithiophilic 3D porous CuZn current collector for stable lithium metal batteries, *ACS Energy Lett.* 5 (2020) 180–186.
- [44] K. Shen, Z. Wang, X. Bi, Y. Ying, D. Zhang, C. Jin, G. Hou, H. Cao, L. Wu, G. Zheng, Y. Tang, X. Tao, J. Lu, Magnetic field-suppressed lithium dendrite growth for stable lithium-metal batteries, *Adv. Energy Mater.* 9 (2019) 1900260.
- [45] Z. Hou, W. Wang, Q. Chen, Y. Yu, X. Zhao, M. Tang, Y. Zheng, Z. Quan, Hybrid protective layer for stable sodium metal anodes at high utilization, *ACS Appl. Mater. Interfaces* 11 (2019) 37693–37700.
- [46] Y. Zhang, C. Wang, G. Pastel, Y. Kuang, H. Xie, Y. Li, B. Liu, W. Luo, C. Chen, L. Hu, 3D wettable framework for dendrite-free alkali metal anodes, *Adv. Energy Mater.* 8 (2018) 1800635.
- [47] L. Mu, S. Xu, Y. Li, Y.S. Hu, H. Li, L. Chen, X. Huang, Prototype sodium-ion batteries using an air-stable and Co/Ni-Free O<sub>3</sub>-layered metal oxide cathode, *Adv. Mater.* 27 (2015) 6928–6933.
- [48] X. Liu, Y. Tan, T. Liu, W. Wang, C. Li, J. Lu, Y. Sun, A simple electrode-level chemical presodiation route by solution spraying to improve the energy density of sodium-ion batteries, *Adv. Funct. Mater.* 29 (2019) 1903795.